Applied Catalysis B: Environmental 252 (2019) 111–119

Contents lists available at ScienceDirect

Applied Catalysis B: Environmental

journal homepage: www.elsevier.com/locate/apcatb

N-doped defective graphene decorated by strontium titanate as efficient photocatalyst for overall water splitting

Diego Mateo, Ana García-Mulero, Josep Albero*, Hermenegildo García*

Instituto de Tecnología Química, Universitat Politècnica de València-Consejo Superior de Investigaciones Científicas, Avenida de los Naranjos s/n, 46022, Valencia, Spain

ARTICLE INFO

Keywords:
Water splitting
Photocatalysis
Solar fuels
Defective graphene
Metal oxides

ABSTRACT

This manuscript reports the synergic effect for overall water splitting of N-doped defective graphenes obtained from the pyrolysis of biomass wastes, upon deposition at 1 wt% of Al-doped $SrTiO_3$ containing $RhCrO_x$ nanoparticles ($RhCrO_x$/STO:Al) as co-catalyst, exhibiting a photocatalytic activity of 153 mmol of H_2 per g of total photocatalyst and 74 mmol/g of O_2 at 24 h irradiation with UV–vis light reaching an incident photon to hydrogen efficiency of 0.67% at 360 nm. This hybrid N-doped defective graphene-$RhCrO_x$/STO:Al photocatalyst was stable in 4 consecutive photocatalytic runs. The obtained results indicate that just a small amount of $RhCrO_x$/STO:Al acting as co-catalysts supported on N-doped defective graphene is sufficient to enhance significantly its photocatalytic activity, making N-doped graphene suitable for overall splitting.

1. Introduction

Photocatalytic water splitting has been proposed as one of the potential approaches for sustainable and clean hydrocarbon production, since this process aims at the direct conversion of solar energy into chemical energy in the form of H_2 to be used as energy vector. As depicted in Scheme 1 in the photocatalytic water splitting, simultaneous oxidation and reduction taking place upon irradiation of a photocatalyst. The photocatalytic overall H_2O splitting into H_2 and O_2 (see Eqs. 1–4) was first reported by Fujishima and Honda using TiO_2 photoelectrodes [1]. Since then, a large variety of semiconductor materials have been explored as photocatalysts, including $SrTiO_3$, CdS, $BiVO_4$, C_3N_4 and defective graphenes, among others. [2,3] Although a considerable progress has been made in this area, semiconductor-based photocatalysts have not yet achieved production yields high enough to implement this technology commercially, there being still necessary to further improve the photocatalytic efficiency. In most cases, the poor efficiency is a consequence of the wide bandgap and fast recombination kinetics of typical semiconductor oxides. [4–6] Among the various strategies to minimize these drawbacks one of the most efficient methodologies is the formation of heterojunctions by contacting two or more components, obtaining hybrid structures that favor charge separation [7–10]. In a relevant example for the present study, Domen and co-workers have recently reported an outstanding photocatalytic activity for overall water splitting using Al-doped $SrTiO_3$ (STO) semiconductor containing Rh and Cr mixed oxide nanoparticles (NPs). [11,12]

$$h\nu \xrightarrow{photocatalyst} e^- + h^+ \quad (1)$$

$$4H^+ + 4e^- \rightarrow 2H_2 \quad (2)$$

$$2H_2O + 4h^+ \rightarrow O_2 + 4H^+ \quad (3)$$

$$2H_2O \rightarrow 2H_2 + O_2 \quad (4)$$

Graphene, a one atom thick 2D sheet of an indefinite number of sp^2-hybridized carbon atoms in hexagonal arrangement, has recently received considerable attention as absorbent and catalyst due to its unique physical and chemical properties such as high specific surface area, large electrical conductivity, photochemical stability and strong interaction with adsorbed nanoparticles, among others. [13–15] Although most of the reports in photocatalysis use minor proportions of graphene as additive observing an increase in the photocatalytic activity of semiconductor in contact to it, [16–19] recent findings have shown that defective graphenes such as graphene oxide, reduced graphene oxide and doped graphenes, possess intrinsic photocatalytic activity towards water splitting as consequence of the transformation of the graphene sheet from conducting to semiconducting caused by the presence of "*defects*" such as carbon vacancies, holes or heteroatoms, including O or N, among other possibilities. [20–23] It is well established that the introduction, for instance, of oxygenated functional groups in graphene transforms sp^2 into sp^3 carbons and the combination of conductive sp^2 and non-conductive sp^3 domains in the graphene sheet originates the

* Corresponding authors.
E-mail addresses: joalsan@itq.upv.es (J. Albero), hgarcia@qim.upv.es (H. García).

https://doi.org/10.1016/j.apcatb.2019.04.011
Received 20 February 2019; Received in revised form 4 April 2019; Accepted 6 April 2019
Available online 08 April 2019
0926-3373/

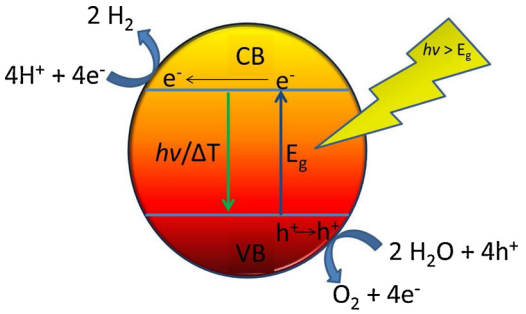

Scheme 1. Fundamental steps in photocatalytic water splitting.

opening of a gap between the conduction and the valence bands. Thus, graphene band gap opening by doping with heteroatoms and introduction of defects has been a general method to convert metallic graphene into a semiconducting material. In this regard, the intrinsic photocatalytic activity for water splitting of defective graphenes obtained from the pyrolysis of biomass wastes, containing in their composition O and N atoms among other defects, has been recently reported. [24,25] Moreover, it was observed that the presence of small amounts of metal or metal oxide NPs greatly improves the photocatalytic performance of these defective graphenes for the overall water splitting in the absence of sacrificial agents. [26,27]

Considering that STO and doped graphenes are among the most efficient photocatalysts for overall water splitting reported so far and the well-stablished synergy of heterojunctions, it appears of interest to determine the photocatalytic activity of a hybrid material combining both components. This work provides a comparison of the photocatalytic activity for overall water splitting of three defective graphenes of different origin and compositions that have been decorated with Al-doped STO modified by $RhCrO_x$ NPs ($RhCrO_x$/STO:Al) as co-catalyst. The selection of $RhCrO_x$/STO:Al and graphenes in this study is motivated by the high photocatalytic activity for overall water splitting of both materials separately and the expected synergy of the heterojunction. It will be demonstrated that the addition of small weight percentages of $RhCrO_x$/STO:Al to the different graphenes promotes the photocatalytic overall water splitting and that the defect concentration on the graphene sheet and its nature play an important role in the observed photocatalytic activity.

2. Experimental

2.1. Materials and procedures

2.1.1. Preparation of G and N-G

While comG was purchased from Strem Chemicals, G and N-G were obtained by pyrolysis at 900 °C under Ar in a horizontal electrical furnace using alginic acid or chitosan as precursors, following reported procedures. In previous reference [28] more details can be found.

2.1.2. Preparation of Al-doped $SrTiO_3$ powder loaded with $RhCrO_x$

The preparation of Al-doped $SrTiO_3$ (STO:Al) was performed using a flux method previously reported by Chiang et al. [11] Briefly, $SrTiO_3$ (Sigma), Al_2O_3 (Sigma) and $SrCl_2$ (Sigma, 99.99%, anhydrous) were mixed in a molar proportion of 1:0.02:10 using an agate mortar. Once the mixture was completely homogenized, it was placed into an alumina crucible and calcined under air at 1150 °C for 10 h at a heating rate of 5 °C/min. The obtained solid was washed with distilled water to remove $SrCl_2$ and soluble impurities and the sample was dried at 40 °C overnight.

The STO:Al powder was loaded with a mixed oxide of Rh and Cr ($RhCrO_x$) at 1 wt% by the impregnation method, as previously reported. $RhCl_3{\cdot}xH_2O$ (Aldrich) and $Cr(NO_3)_3{\cdot}9H_2O$ (Sigma) were used as metal precursors. The STO:Al powder was dispersed in the minimum volume of water and an aqueous solution containing the proper amount of Rh and Cr precursors was added dropwise under continuous stirring at a 55 °C. After evaporating to dryness, the solid was calcined in air at 350 °C for 1 h.

2.1.3. Preparation of $RhCrO_x$/STO:Al-loaded graphene ($RhCrO_x$/STO:Al/G)

$RhCrO_x$/STO:Al was loaded onto three graphene samples by the impregnation method. Briefly, the graphene sample was dispersed in the minimum volume of water (100 mg/5 mL) using a tip sonicator (750 W) for 1 h. An aqueous solution of $RhCrO_x$/STO:Al with different loadings (0.5–10 mg in 20 mL) was added dropwise to the graphene suspension under continuous stirring. The mixture was heated at 55 °C in order to slowly evaporate the water. After finishing the impregnation of graphene with the $RhCrO_x$/STO:Al, the obtained solid was exhaustively washed with milliQ water and dried.

This was the general procedure to prepare samples of $RhCrO_x$/STO:Al loaded onto three different graphenes: graphene obtained from chitosan ($RhCrO_x$/STO:Al/N-G), graphene from alginic acid ($RhCrO_x$/STO:Al/G) and commercial graphene ($RhCrO_x$/STO:Al/comG) from Strem Chemicals.

2.2. Characterization

The amount of metals present in the samples was determined by inductively coupled plasma-optical emission spectrometry (ICP-OES) by dissolving the photocatalyst with *aqua regia* and analyzing the resulting solution.

Raman spectra were recorded with a Horiba Jobin Yvon-Labram HR UV–vis-NIR (200–1600 nm) Raman Microscope Spectrophotometer, using a 512 nm laser as the excitation source. Raman spectra were obtained averaging 10 scans at a resolution of 2 cm^{-1}.

HRTEM images were recorded in a JEOL JEM 2100 F under 200 kV accelerating voltage. Samples were prepared by casting one drop of the suspended material in ethanol onto a carbon-coated copper TEM grid, and allowing it to dry at room temperature.

Diffuse reflectance UV–vis spectra in the range of 200–800 were recorded on a Cary 5000 spectrophotometer from Varian.

2.3. Photocatalytic tests

Photocatalytic experiments were performed using a 51 mL volume cylindrical quartz reactor. The photocatalyst was dispersed in 25 mL of ultrapure water (1 mg/mL) with an ultrasonicator. After that, it was introduced in the reactor and the atmosphere was purged with an argon flow for 15 min. The reactor was irradiated using a 300 W Xe lamp and the temperature of the reactant solution was maintained at 25 °C by a coupled cooling system. The produced gases were analyzed using an Agilent MicroGC equipped with a Molsieve 5 A column and a TCD detector with argon as the carrier gas.

Values of apparent quantum yield (AQY) were determined under irradiation with a 150 W Xe lamp equipped with a Czerny Turner monochromator. AQY values were calculated using this Eq. (5)

$$AQY = \frac{Number\ of\ evolved\ H_2\ molecules\ x\ 2}{Number\ of\ incident\ photons} \quad (5)$$

2.4. Photocurrent measurements

Photocurrent experiments were performed by preparing FTO electrodes with the different samples under study. The samples, a Pt electrode and a saturated Ag/AgCl electrode acted as working electrode, counter electrode and reference electrode, respectively. 1 M aqueous solution of $LiClO_4$ was used as electrolyte. A 300 W Xe lamp was used as irradiation source. The photocurrent was determined at different light intensities which were measured with a calibrated photodiode.

2.5. Transient absorption measurements

Transient absorption spectra were recorded using the forth harmonic of a Q switched Nd:YAG laser (Quantel Brilliant, 266 nm, 15 mJ/pulse, 7 ns fwhm) coupled to a mLFP-122 Luzchem miniaturized detection equipment. This transient absorption spectrometer includes a 300 W ceramic xenon lamp, 125 mm monochromator, Tektronix TDS-2001C digitizer, compact photomultiplier and power supply, cell holder and fiber-optic connectors, computer interfaces, and a software package developed in the LabVIEW environment from National Instruments. The laser flash generates a 5 V trigger pulses with programmable frequency and delay. The rise time of the detector/digitizer is- 3 ns up to 300 MHz (2.5 GHz sampling). The monitoring beam is provided by a ceramic xenon lamp and delivered through fiber-optic cable. The laser pulse is probed by a fiber that synchronizes the photomultiplier detection system with the digitizer operating in the pretrigger mode.

3. Results and discussion

3.1. Photocatalyst preparation and characterization

Photocatalysts were composed by three different graphenes and the doped semiconductor $RhCrO_x$/STO:Al. Their preparation is illustrated in Scheme 2 and described in detail in the Experimental Section. In brief, chitosan and alginic acid were pyrolized at 900 °C under Ar atmosphere to obtain two defective graphenes containing (N-G) 6.43 wt% N or 0.96 wt% (G) dopant nitrogen, respectively. It is worth commenting that, although alginic acid does not contain N in its chemical composition, its solubilization in water requires neutralization that in the present case has been done with NH_3 forming the corresponding water soluble ammonium alginate salt. Upon pyrolysis, most of the NH_4^+ is decomposed and evolves as NH_3 gas, but a very minor percentage is incorporated in the resulting G sample as dopant. The $RhCrO_x$/STO:Al co-catalyst was prepared separately, as reported before. [11] In the first step, commercial $SrTiO_3$, Al_2O_3 and $SrCl_2$ powders at a 1:0.02:10 M ratio were mixed and molten at 1100 °C to obtain STO:Al. Then, Rh and Cr salts were deposited on STO:Al by incipient wetness impregnation [11] and the resulting composite calcined in air at 350 °C. Finally, the as-prepared $RhCrO_x$/STO:Al particles were adsorbed on N-G, G and a commercial graphene sample (comG), and the hybrid composites exhaustively washed to remove loosely adhered inorganic particles. Thus, following this procedure, three samples having small amounts of $RhCrO_x$/STO:Al dispersed on the different graphenes ($RhCrO_x$/STO:Al/N-G, $RhCrO_x$/STO:Al/G, $RhCrO_x$/STO:Al/comG) were prepared. Table 1 summarized the origin and the main analytical data of the samples under study.

The Raman spectra of N-G and G samples are shown in Fig. 1(a). As can be observed, two prominent peaks corresponding to the characteristic G and D bands observed in defective graphenes were recorded in the three samples at 1590 and 1350 cm^{-1}, respectively. In comparison, comG shows G and D peaks at the same position, but with remarkable narrow width. In addition, while G and N-G samples present a broad band between 2500 and 3200 cm^{-1} corresponding to a distribution of few and multilayer configuration, comG presents again a narrow peak centered at 2700 cm^{-1} attributable to the 2D band. All these Raman features are indicating that comG sample contains significantly lesser defects and is constituted mainly by few-layers graphene, while G and N-G samples contain higher defect density and have a multi-layer configuration.

High resolution XPS was used to investigate the distribution of the N atoms among different possible families on the N-G sample. As can be observed in Fig. 1(b), the high resolution C 1 s peak can be deconvoluted in four main components assigned to sp^2 graphene C, and C atoms bonded to C—N or C—O and C═O and CO_2H groups centered at 284.6 eV, 285.6 eV, 286.3 eV and 289.1 eV, respectively. The distribution of N atoms was also based on the high resolution XPS N 1 s peak for N-G sample (Fig. 1(c)). The experimental data was deconvoluted to two main components attributed to quaternary (32.2%) and pyridinic (67.8%) N atoms at 400.3 eV and 398.3 eV, respectively.

The percentage of heteroatoms on the graphene samples was quantified by combustion elemental analysis and the results are summarized in Table 1. The most salient feature of these analytical data is that all the three graphene samples contain O in its composition in similar percentage for N-G and G and larger proportion for comG. In accordance with reported data and the origin of the graphene, only N-G presents in its composition a notable N content, being this element in low or negligible proportion in the composition of G and comG, respectively.

For the $RhCrO_x$/STO:Al co-catalyst ICP-OES analysis confirmed the presence of Rh, Cr, Sr, Ti and Al, in a percentage of 0.4 wt% for Rh and Cr and 0.005 wt% of Al. Moreover, the final loading of $RhCrO_x$/STO:Al on the three graphenes determined also by the ICP-OES analysis, was in accordance with the almost complete adsorption of $RhCrO_x$/STO:Al on the graphene samples during the deposition step, reaching a loading for the three samples of 1 wt% approximately.

All samples exhibit in TEM the characteristic 2D morphology of

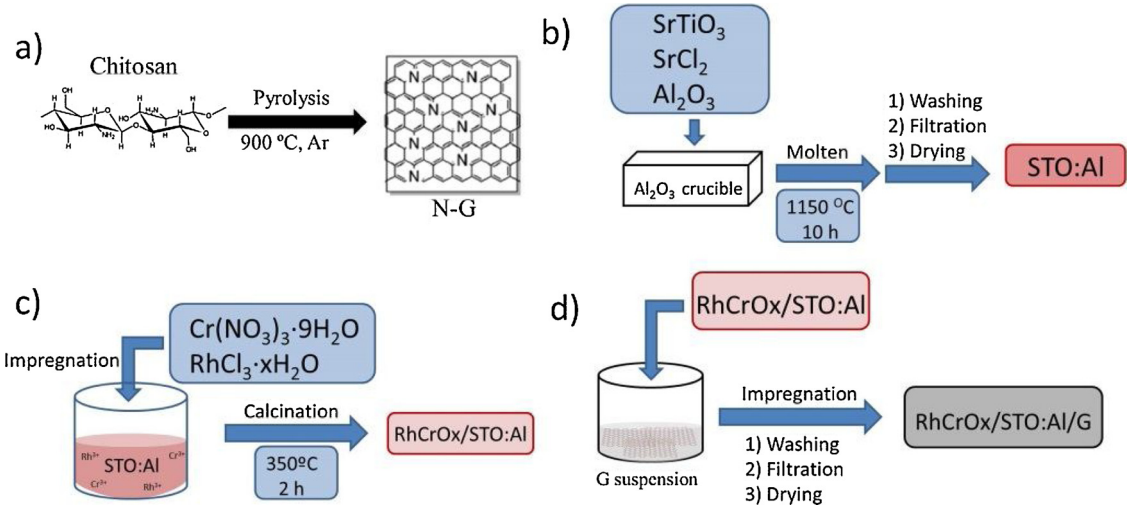

Scheme 2. $RhCrO_x$/STO:Al/N-G photocatalysts preparation method. (a) N-G obtained from chitosan pyrolysis, (b) Al:STO preparation upon molten salts at 1150 °C and subsequent washing, filtration and drying steps, (c) Al:STO impregnation with Cr and Rh salts and calcination at 350 °C, (d) $RhCrO_x$/STO:Al impregnation on the previously prepared N-G and final photocatalyst washing, filtration and drying steps.

Table 1
Origin of the employed graphenes and main analytical data obtained from combustion elemental analysis and ICP-OES of the samples under study.

Samples	Graphene origin	Elemental analysis (wt%)			ICP-OES (wt%)		
		C	O	N	$RhCrO_x$/STO:Al	Rh[a]	Cr[a]
$RhCrO_x$/STO:Al/N-G	Chitosan	84.30	8.27	6.43	1	0.4	0.4
$RhCrO_x$/STO:Al/G	Alginic acid	88.76	9.28	0.96	1	0.4	0.4
$RhCrO_x$/STO:AlcomG	Commercial	85.32	13.68	–	1	0.4	0.4

[a] percentages referred to $RhCrO_x$/STO:Al mass.

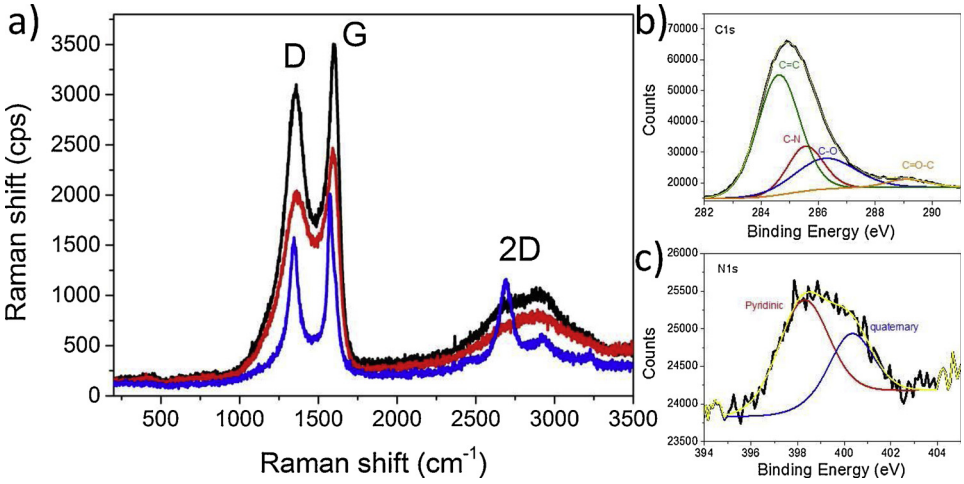

Fig. 1. (a) Raman spectra of G (black), N-G (red) and comG (blue). Laser excitation 514 nm. High resolution XPS for C1 s (b) and N1 s (c) recorded for N-G sample and the best deconvolution for their individual components. (For interpretation of the references to colour in this figure legend, the reader is referred to the web version of this article.)

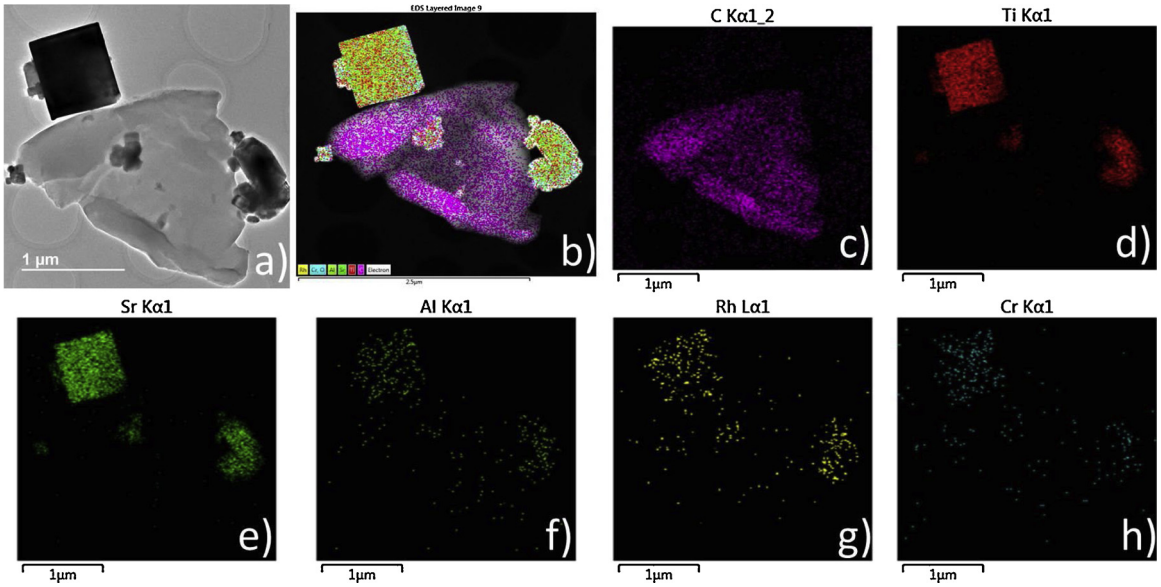

Fig. 2. HRTEM of 1 wt% $RhCrO_x$/STO:Al NPs loaded N-G (a) and elemental analysis for the individual elements (frames c–h) by EDS and overlay (b).

graphenes exhibiting sheets of micrometric size light contrast and wrinkles. These sheets have in contact smaller submicrometric and thicker particles of $RhCrO_x$/STO:Al. To illustrate these observations, Fig. 2 shows a representative HRTEM image of N-G containing 1 wt% of $RhCrO_x$/STO:Al and the corresponding elemental mapping obtained from EDS elemental analysis.

In Fig. 2(a) a graphene sheet can be clearly distinguished with the characteristic laminar morphology exhibiting light contrast and wrinkles indicating the flexibility of the sheet due to its few layers configuration. The average size of these sheets is about 2 µm. The image also shows the presence of $RhCrO_x$/STO:Al particles either on top of the graphene sheets or in close contact characterized by a darker contrast than N-G due to the higher atomic weight of its elements. The particle size distribution of $RhCrO_x$/STO:Al particles appears to be wide, ranging from 100 to 800 nm.

Mapping the different elements detected in the sample observed by HRTEM at submicrometric resolution was performed by EDS. Fig. 2 also presents the corresponding element distribution over the sample for the individual elements and their overlay. This mapping confirms that the 2D particle is composed by C, therefore corresponding to graphene, while the darker particles correspond to $RhCrO_x$/STO:Al. Moreover, EDS was able to detect in the samples the presence of Al, Cr and Rh that are in very low proportion acting as dopant elements in $RhCrO_x$/STO:Al. EDS data are, therefore, in general agreement with ICP-OES

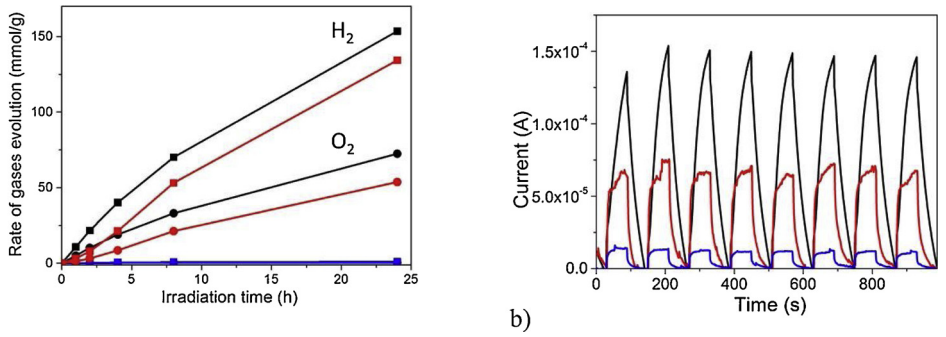

Fig. 3. (a)Temporal evolution of H_2 (squares) and O_2 (dots) in mmol per total photocatalyst mass for $RhCrO_x$/STO:Al/G (red), $RhCrO_x$/STO:Al/N-G (black) and $RhCrO_x$/STO:Al/comG (blue) upon irradiation with a 300 W Xe lamp. (b) Photocurrent measurements of electrodes prepared by depositing $RhCrO_x$/STO:Al/G (red), $RhCrO_x$/STO:Al/N-G (black) and $RhCrO_x$/STO:Al/comG (blue) photocatalysts on FTO (1.5 × 1 cm^2). Electrolyte: 1 M $LiClO_4$ aqueous solution. Eight consecutive cycles of 60 s were carried out switching on and off UV–vis light from a Xe lamp at 1113 W/m^2 irradiation while photocurrent values were acquired. (For interpretation of the references to colour in this figure legend, the reader is referred to the web version of this article.)

analysis and with the homogeneous distribution of this metal oxide dopants over the $SrTiO_3$ particles.

3.2. Photocatalytic tests

The photocatalytic activity towards overall water splitting upon UV–vis irradiation with a 300 W Xe lamp was tested by dispersing 25 mg of the different samples ($RhCrO_x$/STO:Al/G, $RhCrO_x$/STO:Al/N-G and $RhCrO_x$/STO:Al/comG) in MilliQ-water at 1 mg/mL, purging exhaustively with Ar before irradiation. Analysis of the gases was performed by connecting directly the photoreactor to a micro-GC with two columns (Molsieve 5 A and PPQ) and TC detectors that allow to monitor and quantify H_2, O_2, N_2, CO_2, CO and < C_3 hydrocarbons. Gas evolution from aqueous dispersions of the three different hybrid composites over the irradiation time is shown in Fig. 3(a). Note that no sacrificial electron donor was used in these experiments. Control experiments using N-G, G and comG as photocatalysts in the absence of $RhCrO_x$/STO:Al were carried out for overall water splitting. Under these conditions, the observed H_2 as O_2 evolution at 24 h was in the detection limit of our micro-GC corresponding to H_2 values about 5 magnitude orders lower than the amount observed when $RhCrO_x$/STO:Al co-catalyst is loaded on the different graphenes. Similarly, another control experiment using as photocatalyst the amount of $RhCrO_x$/STO:Al present in the hybrid graphenic composites (0.2 mg) did not allow to detect the presence of H_2 or O_2. Additional control experiments in the absence of light, by covering the photoreactor with aluminum foil while the light was on, were also carried out using the different photocatalysts, but undetectable H_2 and O_2 amounts were found, meaning that H_2 and O_2 evolution requires irradiation of the photocatalysts to occur.

As can be observed in Fig. 3(a), only the hybrid samples based on defective graphenes ($RhCrO_x$/STO:Al/G and $RhCrO_x$/STO:Al/ N-G) containing N atoms showed photocatalytic activity towards water splitting, observing the simultaneous evolution of O_2 and H_2 in stoichiometric amounts according to Eq. (4). In contrast, the sample based on comG with less density of defects according to the Raman spectrum presented negligible photocatalytic activity for water splitting under the present conditions. These results are in good agreement with some precedents in the literature showing that the photocatalytic activity in defective graphenes arises from the presence of doping elements and lattice defects that convert them into semiconductor materials, being ideal graphene (containing negligible or a very low defects concentration) photocatalytically inactive or exhibiting much lower photocatalytic activity. [20,29] Thus, while ideal graphene is almost completely transparent in all the UV–vis wavelength range, the presence of dopant heteroatoms or defects introduces a band in the UV region expanding towards the visible that becomes more intense and better defined as the dopant percentage and defect density increases in a certain range [24,25].

It must be commented, however, that no all dopant elements and defects contribute equally to the efficiency of the photocatalytic activity of this reaction. Graphene oxide has been previously used as photocatalysts for water splitting, and it has been reported that the concentration of O atoms in the graphenic lattice influences the oxidation semi-reaction due to valence band shift with the O concentration. [30] In this regard, it has been reported that doping with N affords degective graphenes that exhibit a high photocatalytic activity for hydrogen generation. [25] The photocatalytic activity order shown in Fig. 3 can be easier rationalized based on the compositional differences between the different graphenes, being N-G the one with the highest N content in the graphenic structure, much higher than that of G, while no N is present in comG. This efficiency order is consistent with earlier reports on the influence of N doping on the performance of defective graphenes as hydrogen generation photocatalysts. Thus, the H_2 and O_2 production after 24 h reaction using $RhCrO_x$/STO:Al/N-G as photocatalyst was of 153.6 mmol/g and 72.4 mmol/g, respectively. Although still notably active, lower amounts of H_2 and O_2, 134.2 and 53.7 mmol/g, respectively, were measured at 24 h when $RhCrO_x$/STO:Al/G was used under the same reaction conditions. Previous reports have described the H_2 evolution from water using N- and P-doped graphenes as photocatalysts in the presence of sacrificial electron donors (MeOH, triethanolamine (TEOA), etc.) [24,25]. It was demonstrated that the H_2 production was affected by the concentration of heteroatoms in the graphene.

Overall our results are in good agreement with the related reported data in the sense of the beneficial influence of N for the photocatalytic activity. These experimental data are also in accordance with theoretical calculations that have proposed that the bandgap opening increases with the loading of N up to a certain value about 8 wt%. Calculations predict that no much influence of further additional N atom loading should be reflected on the bandgap beyond this value [31]. According to these theoretical calculations, it is in the range from 0 to about 8 wt% where remarkable differences in the photocatalytic activity of the N-doped graphenes should be expected and the present results with three graphene samples with a range of N content are in nice agreement with these predictions.

Regarding the important role of $RhCrO_x$/STO:Al, it should be reminded that both components independently either do not exhibit photocatalytic activity (case of $RhCrO_x$/STO:Al) or it is very minor (case of N-G) under the present operating conditions. Therefore, considering the low weight percent of $RhCrO_x$/STO:Al in the samples under study it is proposed that the $RhCrO_x$/STO:Al role is to act as co-catalysts favoring charge separation and gas evolution. It is well-established that co-catalysts have a remarkable effect at low loadings as it is the present case.

To determine the photoresponse of the three samples, photocurrent measurements were carried out. Three different photoelectrodes were fabricated depositing identical amounts of the photocatalysts on transparent fluorine-doped tin oxide (FTO) transparent electrode. The

photoelectrode fabrication procedure is described in the experimental section in 2.4 Photocurrent Measurements. The results of the photoresponse measurements are presented in Fig. 3(b).

The photocurrent measured for the three samples follows the same trend that the photocatalytic activity showed in Fig. 3(a). Although all the photoelectrodes presented a notable stability after eight consecutive cycles, the temporal profiles present significant differences depending on the photocatalyst. In the case of $RhCrO_x$/STO:Al/N-G a built up of charge indicative of a capacitative accumulation of charges in the film was observed. This behavior is associated with a large charge carrier density with limited mobility in the layer associated to lower electrical conductivity. Thus, while $RhCrO_x$/STO:Al/comG, presenting the lowest photocurrent, reached the maximum current value in a very short period of time indicating high electrical conductivity, $RhCrO_x$/STO:Al/N-G, which exhibits the higher photoresponse, presents a gradual current growth over the time, achieving under our cycling conditions the maximum current value at the moment the light was going to be switched off (100 s). From this point, the current decrease was also not instantaneous, but gradual. In this way, upon photoelectrode irradiation a build up of charge carriers with low mobility is taking place, and, the current flow increases gradually with the potential of the electrode during the irradiation period. When the light is switched off, the opposite behavior, i.e., the capacitor discharge occurs prolonging the current long after the light was off. Since all photoelectrodes were prepared under identical conditions, this capacitative behavior can be attributed to the intrinsic electrical properties of $RhCrO_x$/STO:Al/N-G film that are more remarkable than those of the other two samples, reflecting again the influence of the N content on the photoelectrochemical performance of the hybrid material.

3.3. Mechanism

To gain further understanding on the nature and lifetime of the photogenerated charge separation state transient absorption measurements in the microsecond time scale were carried out in Ar-purged acetonitrile dispersions of RhCrOx/STO:Al/N-G at 0.1 mg/ml, and compared the signal with those of independent RhCrOx/STO:Al and N-G samples as references. All samples were excited at 355 nm with the third harmonic of a Nd:YAG laser and the excited state decay kinetics was monitored at 440 nm. The results are presented in Fig. 4. The excited state of RhCrOx/STO:Al exhibited the shortest lifetime decaying following a single exponential kinetics with τ of 389 ns. On the other hand, the excited state decay of N-G can be fitted adequately to bi-exponential kinetics, showing a fast component with lifetime of 481 ns and a contribution of 80% and a slow-component with lifetime of 3.41 μs. This bi-exponential kinetics monitored for N-doped graphene excited state agrees with reported studies in the literature. [32,33] The temporal profile of the signal corresponding to RhCrOx/STO:Al/N-G excited state exhibits notable differences respect to the two components exhibiting also a bi-exponential kinetics with a fast component of 345 ns accounting for 75%, similarly to the one measured for N-G. However, the slow component showed remarkably a much extended lifetime of 22.06 μs. The overall signature of the RhCrOx/STO:Al/N-G transient state indicates, on one hand, that the excited state of the composite is mainly localized on N-G. This is reasonable considering the much higher proportion of N-G over RhCrOx/STO:Al. In this way, the behavior of RhCrOx/STO:Al/N-G is in general terms similar to that of N-G. Also the transient absorption spectra of RhCrOx/STO:Al/N-G and N-G consisting in a continuous absorption all over the wavelength range are very similar for both materials and different from that of RhCrOx/STO:Al, measured at 1 μs and 200 ns, respectively. (Fig. 4(ii)). What is important from the photocatalytic activity point of view is that the lifetime of the slow component of the excited state of RhCrOx/STO:Al/N-G is much larger, providing spectroscopic evidence that when the RhCrOx/STO:Al acting as co-catalyst is supported on N-G the charge separation state become longer.

The influence of the $RhCrO_x$/STO:Al loading on the photocatalystic activity was also studied. To address this point, three additional samples of N-G containing different $RhCrO_x$/STO:Al loadings from 0.1 to 6.5 wt% were prepared and their photocatalytic activity measured. These results are in shown Fig. 5(a).

As it can be observed there, the photocatalytic activity of $RhCrO_x$/STO:Al/N-G increased somewhat with the $RhCrO_x$/STO:Al loading up to 1 wt%. Further increase in the $RhCrO_x$/STO:Al loading on N-G produced a notable detrimental effect in the water splitting reaction, decreasing the activity for H_2 evolution over one order of magnitude when that loading was 6.5 wt%. The behavior shown in Fig. 5(a) is typical for a mechanism in which $RhCrO_x$/STO:Al is acting as co-catalyst, increasing the activity of N-G with loading up to the point in which most of the photogenerated charge carriers are being trapped by the co-catalyst. Beyond this point, higher co-catalyst loadings are detrimental due the promotion of charge recombination, screen effect as light absorption, aggregation and increase in the co-catalyst particle size, high surface coverage among other possible negative effects.

On the other hand, in order to further investigate the role of the $RhCrO_x$ and Al dopants contained in the $RhCrO_x$/STO:Al co-catalyst, an analogous hybrid sample was prepared impregnating plain STO on N-G at 1 wt% loading. Then, the photocatalytic activity of STO/N-G towards overall water splitting was investigated. After 24 h illumination in milli-Q water, the H_2 and O_2 amounts were below the Micro-GC detection limit, indicating that, in spite of the small amount of Rh, Cr and Al (0.4, 0.4 and 0.005 wt%, respectively), they have an important role in the activity of the $RhCrO_x$/STO:Al/N-G photocatalyst. It has been previously reported that semiconductor doping is a convenient method to introduce mid-gap states in semiconductors that causes band gap decrease. [34] In the present case, the incorporation of Al and $RhCrO_x$ dopants produce a visual color change of STO from white to light orange, indicating a band gap reduction. Tauc plots of STO and $RhCrO_x$/STO:Al obtained from their diffuse reflectance UV-Vis spectra confirm the STO band gap reduction from 3.3 to 3.08 eV upon semiconductor

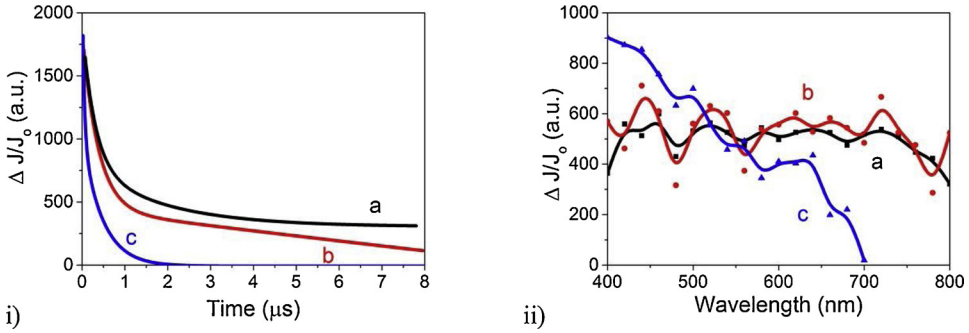

Fig. 4. Transient signal decays monitored at 440 nm (i) and spectra (ii) of $RhCrO_x$/STO:Al/N-G (a), N-G (b) and $RhCrO_x$/STO:Al (c). Excitation wavelength 355 nm. ii: Transient absorption spectra of $RhCrO_x$/STO:Al/N-G (a) and N-G (b) acquired at 1 μs and transient absorption spectrum of $RhCrO_x$/STO:Al (c) acquired at 200 ns.

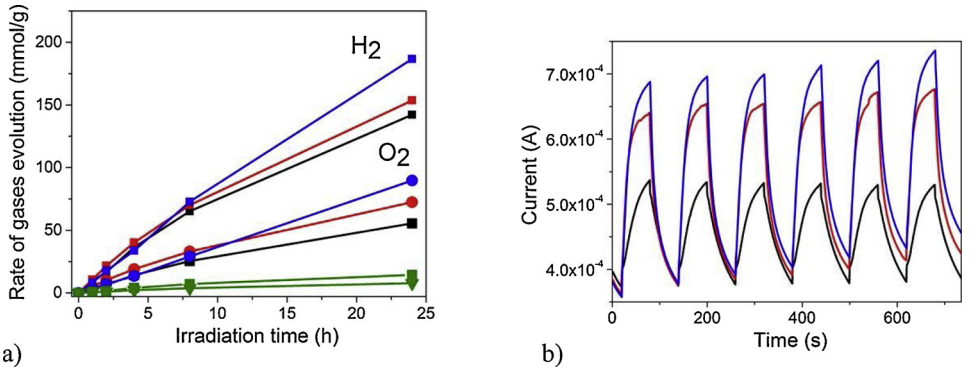

Fig. 5. (a) H_2 (squares) and O_2 (dots) evolution using $RhCrO_x$/STO:Al/ N-G as photocatalyst containing 0.1 wt% (black), 0.2 wt% (red), 1 wt % (blue) and 6.5 wt% (green) $RhCrO_x$/STO:Al loading. Photocatalysts were dispersed at 1 mg/mL in Ar-purged MilliQ water (25 ml) by sonication and irradiated upon UV–vis light from a Xe lamp (1113 W/m^2). Total photocatalysts mass 25 mg. (b) Photocurrent measurements at different light intensities using the $RhCrO_x$/STO:Al/N-G photocatalysts (1 wt% loading of $RhCrO_x$/STO:Al) deposited on FTO: 1298 (black), 1790 (red) and 3341 (blue) W/m^2. (For interpretation of the references to colour in this figure legend, the reader is referred to the web version of this article.)

doping (see Fig. S1 in Supplementary Information). Moreover, when the photocatalytic activity of an aqueous STO/N-G dispersion was measured in the presence of triethanolamine (15 vol%.) as sacrificial electron donor, a H_2 production rate of 34.2 μmol/g·h was obtained, indicating that H_2 evolution (Eq. 2) can still take place in the absence of the Al and $RhCrO_x$ dopants. However, the fact that STO/N-G did not promote overall water splitting indicates that the H_2O oxidation (Eq. 3) cannot occur in the absence of the Al and $RhCrO_x$ dopants. Therefore, the dopants role in the $RhCrO_x$/STO:Al/N-G co-catalyst appears to be the introduction of mid-gap states in the STO semiconductor and the catalytic activity to promote the H_2O oxidation reaction in $RhCrO_x$/STO:Al co-catalyst. These finding are in good agreement with the original repots in this modified perovskite as intrinsic photocatalyst. It should be remarked that the preparation of $RhCrO_x$ NPs directly adsorbed in N-doped defective graphene is not possible since, as reported in the experimental section, formation of mixed Rh and Cr oxide NPs after impregnation of the support requires a calcination step in the presence of moisture. Thus, the conditions of the direct grafting on graphene of $RhCrO_x$ NPs would cause graphene combustion due to the aerobic conditions.

To determine the possible positive contribution of direct photoexcitation of $RhCrO_x$/STO:Al in the composite photocatalyst, the diffuse reflectance UV–vis spectra of $RhCrO_x$/STO:Al, N-G and $RhCrO_x$/STO:Al/N-G, containing 1 wt% of the co-catalyst, were recorded. They are shown in Fig. S2 of Supplementary Information. As can be seen there, the absorption spectrum of $RhCrO_x$/STO:Al/N-G appeared to be a sum of the N-G and $RhCrO_x$/STO:Al spectra. It is worth commenting that, in spite of the small amount of $RhCrO_x$/STO:Al deposited onto N-G, the prominent band between 280 and 380 nm corresponding to the doped inorganic semiconductor is clearly observed when this material is decorating the graphene sheets. This high contribution of light absorption by $RhCrO_x$/STO:Al in the UV region is also consequence of the low absorptivity of defective graphenes, ideal graphenes exhibiting a transmittance about 99% of light in all the UV–vis region. The spectral response of $RhCrO_x$/STO:Al/N-G has been investigated measuring the photocatalytic activity upon irradiation using a 360 nm and 400 nm cut-off filters (meaning that UV wavelengths shorter than these numbers are removed and mostly visible radiation illuminates the photocatalyst in these experiments). The results are shown in Fig. S3 in Supplementary Information. As can be seen there, the H_2 production upon Xe lamp irradiation with a 360 nm cut-off filter reaches a 14% of the value obtained with full light illumination, and when a 400 nm cut-off filter was used negligible H_2 production was measured. This is indicating that the main photoresponse of this photocatalyst is taking place bellow 360 nm, and only a 14% production is due to photons emitted between 360 and 400 nm.

The quantum yield of the three photocatalysts at 360 nm was calculated based on the H_2 produced irradiating with monochromatic light. The values obtained at this wavelength were 0.67, 0.17 and 0.03 % for $RhCrO_x$/STO:Al/N-G, $RhCrO_x$/STO:Al/G and $RhCrO_x$/STO:Al/comG, respectively. These values are comparable to other incident photon to hydrogen conversions efficiencies reported in the literature for overall water splitting with stoichiometric generation of H_2 and O_2 and rank the present $RhCrO_x$/STO:Al/N-G among the best photocatalysts for overall water splitting, particularly considering that 99% of the material is based on defective graphene from biomass waste origin. To put the photocatalytic activity of $RhCrO_x$/STO:Al/N-G into context, it should be reminded that carbon nitrides have not enough oxidation potential to perform water oxidation and that the vast majority of studies on the photocatalytic activity for hydrogen generation of graphenes employ sacrificial electron donors, and do not provide information of the activity for overall water splitting.

In order to study the photoresponse of $RhCrO_x$/STO:Al/N-G with the light intensity, photoelectrodes of $RhCrO_x$/STO:Al/N-G supported on FTO were prepared and exposed to irradiation at different light intensities. The results are presented in Fig. 5(b). The measured photocurrent in the $RhCrO_x$/STO:Al/N-G photoelectrodes increased with the irradiation power, although this current increase was not linear and as expected a saturation effect occurs. While the photocurrent increased proportionally when the light irradiation raised from 1298 to 1790 W/m^2, further increase in the light intensity at 3341 W/m^2 produced just a moderate photocurrent increase. Photocurrent saturation indicates that there is a limitation in the amount of charge carriers that can be generated in a material and once a large percentage of this maximum amount of carriers has been generated, further, light intensity does not produce additional effect. In addition, the photoresponse shown in Fig. 5(b) confirms the stability of the photoelectrode response after successive light on/off cycles, as well as the capacitative behavior of this photoelectrode.

3.4. Stability

Finally, the photocatalytic stability of $RhCrO_x$/STO:Al/N-G for overall water splitting was studied performing series of consecutive reuses of the same sample. Photocatalytic stability studies are particularly relevant in the case of graphene materials, since due to their composition they have to be always checked to determine their stability. In these recycling experiments, the $RhCrO_x$/STO:Al/N-G photocatalyst was dispersed in MilliQ water, Ar purged and exposed to UV–vis light irradiation for 4 h periods. During each cycle, the gases evolved were continuously measured. Each new cycle starts with thorough Ar purging of the system to remove completely the H_2 and O_2 produced in the previous run prior to a subsequent 4 h irradiation test. This procedure was repeated 3 additional times. The temporal gas evolution in the 4 consecutive cycles are presented as Fig. 6.

As it can be seen there the stability test shows a slight decrease in the photocatalytic activity after the first run based on the initial rate of H_2 and O_2 evolution and on the gas production after 4 h final time. However, from the second use the initial reaction rates and final gas production remained significantly constant in the consecutive runs.

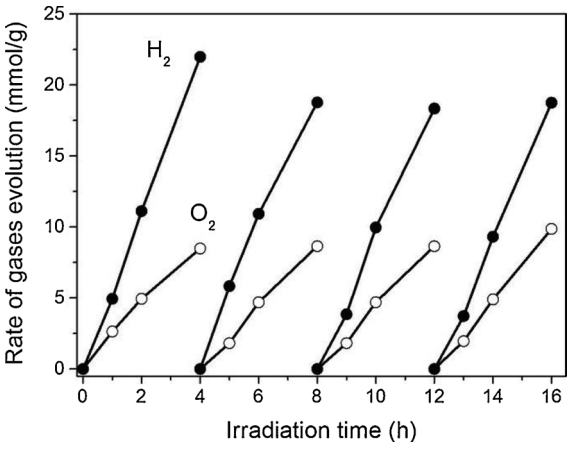

Fig. 6. H_2 (dots) and O_2 (circles) evolution using $RhCrO_x$/STO:Al/N-G photocatalyst dispersed in MilliQ water at 1 mg/mL concentration upon 300 W Xe lamp irradiation (1113 W/m^2) after several Ar purging cycles. Total photocatalysts mass 25 mg.

Moreover, regarding the O_2 evolved during these experiments, its production followed the expected stoichiometry, exhibiting also constant rates and final production yields.

4. Conclusions

In summary, the data provided here have shown that defective N-doped graphene decorated with $RhCrO_x$/STO:Al is a suitable photocatalyst to promote overall water splitting. Among the studied graphenes, N-G, obtained from the pyrolysis of chitosan and containing approximately 6.4 wt% of N in its composition and conveniently decorated by $RhCrO_x$/STO:Al (1 wt%) has exhibited the highest photocatalytic activity reaching 153 mmol/g of H_2 and 74 mmol/g of O_2 from water and light after 24 h irradiation with UV–vis light with an incident photon to hydrogen efficiency of 0.67% at 360 nm. In contrast, the photocatalytic activity obtained from comG, containing the same $RhCrO_x$/STO:Al co-catalyst loading, but lacking N atoms in its composition, was significantly lower. The co-catalyst loading optimization shows that minute amounts (up to 1 wt%) of the doped semiconductor $RhCrO_x$/STO:Al are enough to enhance the photocatalytic activity of defective graphenes towards overall water splitting. Moreover, the role of the Al and $RhCrO_x$ in the co-catalyst has been found to introduce mid-gap states in the STO semiconductor and catalyze water oxidation semi-reaction. $RhCrO_x$/STO:Al/N-G has demonstrated to be stable in 4 consecutive photocatalytic runs or 8 photoresponse cycles. The $RhCrO_x$/STO:Al/N-G photoelectrodes presented a notable capacitative behavior, accumulating charge carriers upon irradiation due to the limited charge mobility. In general, the obtained results confirm that just a small amount of $RhCrO_x$/STO:Al acting as co-catalyst supported on N-doped defective graphene can significantly enhance their photocatalytic activity, making these materials suitable for overall splitting.

Acknowledgments

Financial support by the Spanish Ministry of Economy and Competitiveness (Severo Ochoa, and CTQ2015-69563-CO2-R1) and by the Generalitat Valenciana (Prometeo 2017-083) is gratefully acknowledged. J. A. thanks the Universitat Politècnica de València for a postdoctoral scholarship. D. M. also thanks Spanish Ministry of Science for PhD Scholarship.

Appendix A. Supplementary data

Supplementary material related to this article can be found, in the online version, at doi:https://doi.org/10.1016/j.apcatb.2019.04.011.

References

[1] A. Fujishima, K. Honda, Electrochemical photolysis of water at a semiconductor electrode, Nature 238 (1972) 37.
[2] S. Chen, T. Takata, K. Domen, Particulate photocatalysts for overall water splitting, Nat. Rev. Mater. 2 (2017) 17050.
[3] R.D. Tentu, S. Basu, Photocatalytic water splitting for hydrogen production, Curr. Opin. Electrochem. 5 (2017) 56–62.
[4] M. Ni, M.K. Leung, D.Y. Leung, K. Sumathy, A review and recent developments in photocatalytic water-splitting using TiO2 for hydrogen production, Renewable Sustain. Energy Rev. 11 (2007) 401–425.
[5] S.D. Tilley, M. Cornuz, K. Sivula, M. Grätzel, Light-induced water splitting with hematite: improved nanostructure and iridium oxide catalysis, Angew. Chem. Int. Ed. 49 (2010) 6405–6408.
[6] B. Cole, B. Marsen, E. Miller, Y. Yan, B. To, K. Jones, M. Al-Jassim, Evaluation of nitrogen doping of tungsten oxide for photoelectrochemical water splitting, J. Phys. Chem. C 112 (2008) 5213–5220.
[7] J. Du, X. Lai, N. Yang, J. Zhai, D. Kisailus, F. Su, D. Wang, L. Jiang, Hierarchically ordered macro − mesoporous TiO2 − graphene composite films: improved mass transfer, reduced charge recombination, and their enhanced photocatalytic activities, ACS Nano 5 (2010) 590–596.
[8] X. She, J. Wu, H. Xu, J. Zhong, Y. Wang, Y. Song, K. Nie, Y. Liu, Y. Yang, M.T.F. Rodrigues, High efficiency photocatalytic water splitting using 2D α-Fe2O3/g-C3N4 Z-Scheme catalysts, Adv. Energy Mater. 7 (2017) 1700025.
[9] R.C. Pawar, S. Kang, S.H. Ahn, C.S. Lee, Gold nanoparticle modified graphitic carbon nitride/multi-walled carbon nanotube (gC 3 N 4/CNTs/Au) hybrid photocatalysts for effective water splitting and degradation, RSC Adv. 5 (2015) 24281–24292.
[10] Y. Yang, E. Liu, H. Dai, L. Kang, H. Wu, J. Fan, X. Hu, H. Liu, Photocatalytic activity of Ag–TiO2-graphene ternary nanocomposites and application in hydrogen evolution by water splitting, Int. J. Hydrogen Energy 39 (2014) 7664–7671.
[11] T.H. Chiang, H. Lyu, T. Hisatomi, Y. Goto, T. Takata, M. Katayama, T. Minegishi, K. Domen, Efficient photocatalytic water splitting using Al-doped SrTiO3 coloaded with molybdenum oxide and rhodium–chromium oxide, ACS Catal. 8 (2018) 2782–2788.
[12] Y. Ham, T. Hisatomi, Y. Goto, Y. Moriya, Y. Sakata, A. Yamakata, J. Kubota, K. Domen, Flux-mediated doping of SrTiO 3 photocatalysts for efficient overall water splitting, J. Mater. Chem. A 4 (2016) 3027–3033.
[13] K.S. Novoselov, A.K. Geim, S. Morozov, D. Jiang, M. Katsnelson, I. Grigorieva, S. Dubonos, A.A. Firsov, Two-dimensional gas of massless Dirac fermions in graphene, nature 438 (2005) 197.
[14] A.C. Neto, F. Guinea, N.M. Peres, K.S. Novoselov, A.K. Geim, The electronic properties of graphene, Rev. Mod. Phys. 81 (2009) 109.
[15] Y. Zhu, S. Murali, W. Cai, X. Li, J.W. Suk, J.R. Potts, R.S. Ruoff, Graphene and graphene oxide: synthesis, properties, and applications, Adv. Mater. 22 (2010) 3906–3924.
[16] P. Cheng, Z. Yang, H. Wang, W. Cheng, M. Chen, W. Shangguan, G. Ding, TiO2–graphene nanocomposites for photocatalytic hydrogen production from splitting water, Int. J. Hydrogen Energy 37 (2012) 2224–2230.
[17] X.-J. Lv, W.-F. Fu, H.-X. Chang, H. Zhang, J.-S. Cheng, G.-J. Zhang, Y. Song, C.-Y. Hu, J.-H. Li, Hydrogen evolution from water using semiconductor nanoparticle/graphene composite photocatalysts without noble metals, J. Mater. Chem. 22 (2012) 1539–1546.
[18] X. An, K. Li, J. Tang, Cu2O/reduced graphene oxide composites for the photocatalytic conversion of CO2, ChemSusChem 7 (2014) 1086–1093.
[19] Q. Xiang, J. Yu, M. Jaroniec, Preparation and enhanced visible-light photocatalytic H2-production activity of graphene/C3N4 composites, J. Phys. Chem. C 115 (2011) 7355–7363.
[20] T.F. Yeh, C.Y. Teng, S.J. Chen, H. Teng, Nitrogen-doped graphene oxide quantum dots as photocatalysts for overall water-splitting under visible light Illumination, Adv. Mater. 26 (2014) 3297–3303.
[21] T.F. Yeh, J.M. Syu, C. Cheng, T.H. Chang, H. Teng, Graphite oxide as a photocatalyst for hydrogen production from water, Adv. Funct. Mater. 20 (2010) 2255–2262.
[22] Z. Mou, Y. Wu, J. Sun, P. Yang, Y. Du, C. Lu, TiO2 nanoparticles-functionalized N-doped graphene with superior interfacial contact and enhanced charge separation for photocatalytic hydrogen generation, ACS Appl. Mater. Interfaces 6 (2014) 13798–13806.
[23] M. Xing, W. Fang, X. Yang, B. Tian, J. Zhang, Highly-dispersed boron-doped graphene nanoribbons with enhanced conductibility and photocatalysis, Chem. Commun. 50 (2014) 6637–6640.
[24] M. Latorre-Sánchez, A. Primo, H. García, P-doped graphene obtained by pyrolysis of modified alginate as a photocatalyst for hydrogen generation from water–methanol mixtures, Angew. Chem. Int. Ed. 52 (2013) 11813–11816.
[25] C. Lavorato, A. Primo, R. Molinari, H. Garcia, N-doped graphene derived from biomass as a visible-light photocatalyst for hydrogen generation from water/methanol mixtures, Chem. Eur. J. 20 (2014) 187–194.
[26] D. Mateo, I. Esteve-Adell, J. Albero, J.F.S. Royo, A. Primo, H. Garcia, 111 oriented gold nanoplatelets on multilayer graphene as visible light photocatalyst for overall water splitting, Nat. Commun. 7 (2016) 11819.
[27] D. Mateo, I. Esteve-Adell, J. Albero, A. Primo, H. García, Oriented 2.0. 0 Cu2O nanoplatelets supported on few-layers graphene as efficient visible light photocatalyst for overall water splitting, Appl. Catal. B 201 (2017) 582–590.

[28] A. Primo, P. Atienzar, E. Sanchez, J.M. Delgado, H. García, From biomass wastes to large-area, high-quality, N-doped graphene: catalyst-free carbonization of chitosan coatings on arbitrary substrates, Chem. Commun. 48 (2012) 9254–9256.
[29] Y. Ito, W. Cong, T. Fujita, Z. Tang, M. Chen, High catalytic activity of nitrogen and sulfur co-doped nanoporous graphene in the hydrogen evolution reaction, Angew. Chem. 127 (2015) 2159–2164.
[30] Josep Albero, Diego Mateo, H. García, Graphene-based materials as efficient photocatalysts for water splitting, Molecules 24 (2018).
[31] P. Rani, V. Jindal, Designing band gap of graphene by B and N dopant atoms, RSC Adv. 3 (2013) 802–812.
[32] M.K. Barman, B. Jana, S. Bhattacharyya, A. Patra, Photophysical properties of doped carbon dots (N, P, and B) and their influence on electron/hole transfer in carbon dots–nickel (II) phthalocyanine conjugates, J. Phys. Chem. C 118 (2014) 20034–20041.
[33] H.G. Baldoví, M. Álvaro, B. Ferrer, H. García, Photoinduced charge separation on the microsecond timescale in graphene oxide and reduced graphene oxide suspensions, ChemPhysChem 17 (2016) 958–962.
[34] R. Konta, T. Ishii, H. Kato, A. Kudo, Photocatalytic activities of noble metal ion doped SrTiO3 under visible light irradiation, J. Phys. Chem. B 108 (2004) 8992–8995.